TAO, Vol. 8, No. 2, 221-231, June 1997

Ionospheric Observations of the Solar Eclipse on Oct. 24, 1995 at Chung-Li

Lung-Chih Tsai[1, 2] and Jann-Yenq Liu[2, 1]

(Manuscript received 1 October 1996, in final form 13 March 1997)

ABSTRACT

The main purpose of this paper is to illustrate the usefulness of ionosonde observations in the study of the effects due to the transit of a solar eclipse. A sequence of ionograms were obtained during the eclipse on October 24, 1995 by the Chung-Li Digisonde (situated at 24.9°N, 121.5°E, 35.2°N magnetic dip). With fuzzy classification techniques being used, an algorithm was devised to automatically scale digital ionograms. In corresponding time, significant depletions of *foE* and *foF1* were observed and were indicative of a response to the eclipse effect. Furthermore, a search for the production of atmospheric gravity waves (AGW) induced by the solar eclipse was investigated using the iso-frequency virtual height profiles with time. Time-frequency spectral analysis using the Wigner-Ville distribution was applied to obtain an AGW with a period of 18.5 min in the *F1*- and the lower part of the *F2*-layers. The induced AGW began at the start of the solar eclipse and ended a couple of hours after the completion of the eclipse. In contrast, the iso-frequency profiles with time were also spectrally analyzed with the maximum entropy method (MEM).

(Key words: Solar eclipse, Ionospheric observation, Atmospheric gravity waves, Ionosonde)

1. INTRODUCTION

Ionospheric eclipse observations make valuable contributions to study the transient properties of ionizing radiation from the Sun and to explore chemical and transport processes in the ionosphere. In a number of papers, experimental and theoretical eclipse results have been compared to derive the rates of electron production and the loss of ionization. It is well known that a solar eclipse decreases the electron density in the E, F1 and the lower part of the F2-layer. The critical frequency in the F2-region is more related to transport and thermal pro-

[1]Center for Space and Remote Sensing Research, National Central University, Chung-Li, Taiwan, R.O.C.

[2]Graduate Institute of Space Science, National Central University, Chung-Li, Taiwan, R.O.C.

cesses. More recent investigations have been concerned with the search for atmospheric gravity waves induced by a solar eclipse. Chimonas and Hines (1970) suggested that as the lunar shadow sweeps at supersonic speed across the Earth, the cooling atmosphere acts as a continuous source of gravity waves and builds up a bow wave. The first observation of an induced gravity wave signature in the form of column electron content fluctuations was reported by Davis and da Rosa (1970). Their observations indicated an oscillatory disturbance with a quasi period of about 20 min at about the time predicted for the arrival of atmospheric gravity waves due to the solar eclipse of March 7, 1970. However, Davies (1982) reviewed the reported experimental evidence and concluded that their direct relationship had not been proven satisfactorily. Walker *et al.* (1991) later showed direct evidence for the induced atmospheric gravity wave (AGW) by a solar eclipse and obtained a period of 30-33 min. Using the same spectral analysis technique of the maximum entropy method (MEM) (see the review by Ulrych and Bishop, 1975), as that in the work done by Walker *et al.* (1991), Cheng (1993) also observed the production of an eclipse AGW but obtained a different period of 17-23 min at the same observatory in Chung-Li.

This paper aims at illustrating the usefulness of ionosonde observations in the study of the ionospheric effects due to the transit of a solar eclipse. To obtain ionospheric parameters, an automatic ionogram scaling algorithm incorporating a fuzzy segmentation method is presented in Section 2. This algorithm is applicable to ionograms recorded by modern digital ionosondes, measuring echo amplitude, pulse group delay and wave polarization as the input information. The scaled parameters *foE*, *foF1*, *foF2* and *hpF2* on the eclipse day are shown and compared to the results obtained on the days both before and after the solar eclipse. In Sections 3 and 4, the techniques of time-frequency analysis based on the Wigner-Ville distribution (WVD) are introduced to the spectral analysis of iso-frequency virtual height profiles with time. Using the non-stationary characteristics of the induced AGW by the solar eclipse, the authors have determined a period of 18.5 min to the induced AGW.

2. IONOSONDE SOUNDING RESULTS

The eclipse of October 24, 1995 at Chung-Li began at 0320 UT (1120 LT), reached a peak of 53% disk obscuration at 0433 UT (1233 LT) and ended at 0546 UT (1346 LT). Rapid sequence ionograms above the Chung-Li Digisonde Observatory (situated at 24.9°N, 121.5°E, 35.2°N magnetic dip) were obtained at 5-min intervals. The digisonde, an advanced digital ionosonde (Bibl and Reinisch, 1978; Reinisch 1986), can measure the following parameters: (1) group travel time of h'; (2) echo amplitude; (3) phase; (4) Doppler frequency; (5) angle of arrival; (6) wave polarization, that is, separation of ordinary and extraordinary waves; and (7) wave-front curvature. The range is measured by the synchronization of the transmitter pulse and sampling time and has a resolution of 2.5 or 5 km. The information on amplitude was obtained by coherent integration between 16 and 256 quadrature samples in 1/2 dB steps. To scale ionospheric parameters on the solar eclipse day, a method for the automatic identification of ionograms traces using fuzzy classification techniques was previously used (Tsai *et al.*, 1996). A measure of the continuity or discontinuity between ionospherically reflected echoes can be obtained using a fuzzy relation that describes a set of rules for echo connectedness.

Based on such measures, the segmentation processing of ionograms can be defined, and their properties are obtained. Segments representing the ordinary and extraordinary reflections from the *E*- and *F*-layers can easily be differentiated from multiple hop echoes. One reason for adding complexity to the identification process stems from the existence of the sporadic *E*-layer (E_s-layer). As a result, the echo traces from the E-region exhibit complex structures on an ionogram when both the *E*- and E_s-layers exist at similar heights and are "fuzzy" connected. It is noted that the corresponding signal amplitude reflected from the E_s-layer is much stronger than normal E-layer echoes. It is purposed that signal amplitude information be used to distinguish the normal *E* trace and the E_s trace from the main E segment. The *E*- and E_s-layer parameters could therefore be scaled. Furthermore, the elimination of multiple E_s echoes connected to the *F*-layer trace could be approached by a similar process using echo amplitude information. The main processing procedures are listed as follows:

(1) interference/stray signals in ionograms are identified and removed;

(2) segment ionograms using a fuzzy continuity technique are obtained;

(3) the main segment is determined as the *F*-layer segment;

(4) the *E*- and E_s-layers are interpreted from the *E*-layer segment;

(5) multiple E_s echoes overlapping to *F*-layer signals are eliminated;

(6) smoothing, extrapolating and interpolating processing of the *F*-layer trace is performed; and

(7) fourteen ionospheric parameters (f_{min}, *foE*, *h'E*, foE_s, type of E_s, fbE_s, *foF1*, *M(3000)F1*, *h'F*, *h'F2*, *foF2*, fxI, and *M(3000)F2)* are determined in the International Union of Radio Science (URSI) IIWG format.

It is well known that in the *E*-region and the lower *F*-region production and loss processes are thought to dominate the variations of electron density. As the disc of the Sun is covered either partially or fully by the Moon during a solar eclipse, the solar flux in each wavelength region is progressively reduced. Figure 1 gives scaled *foE* and *foF1* versus time plots observed on the eclipse day and the days both before and after the solar eclipse. Significant depletions of *foE* and *foF1* in the corresponding time of the eclipse are clearly evident. The foE (*foF1*) was reduced from 3.3 (4.5) MHz to a minimum value of 2.7 (3.8) MHz, but then recovered. Relative to the noneclipse time, the associated electron density was decreased by up to 33% at the eclipse maximum. Furthermore, a time delay of the foF1 minimum with respect to the foE minimum can be observed. The lag of the electron density minimum increases with altitude as might be expected in the E-region and the lower F-region of an eclipse ionosphere. For the *F2*-region, Figure 2 shows *foF2* and *hpF2* profiles with time on the eclipse day and the previous and next 'control' days. It can be deduced that the reduction in *foF2* (referred to the two control days) occurred after the start of the solar eclipse; the maximum reduction in *foF2* was observed not at the time of the eclipse maximum but somewhat later. Additionally, the value of *foF2* decreased in the first half of the eclipse period but increased in the other half; *hpF2* fell when *foF2* increased and rose when *foF2* dropped. In the early eclipse observations, there were no coherent results to show a consistent pattern in the behaviour of *foF2*. Certainly, the effects of transport are important in the ionospheric *F2*-region.

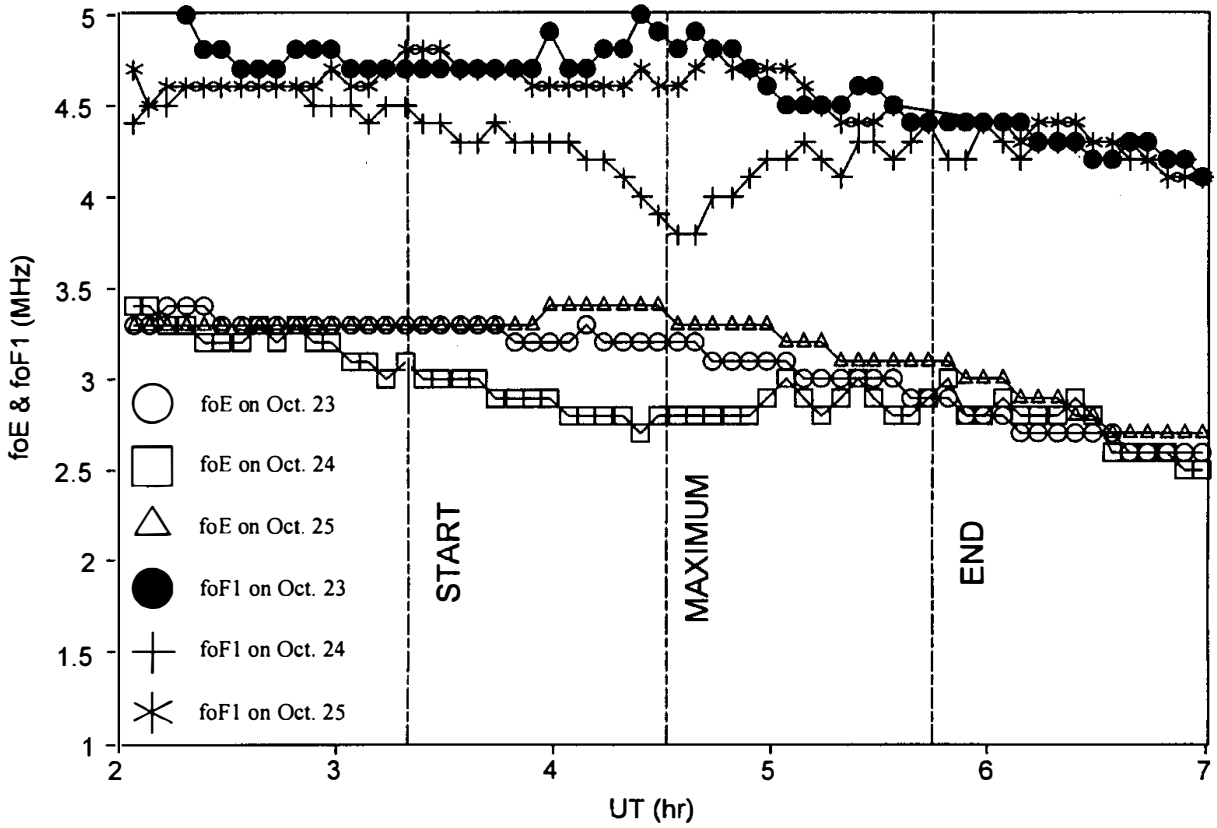

Fig. 1. foE and *foF1* profiles with time on October 23, 24, and 25, 1995.

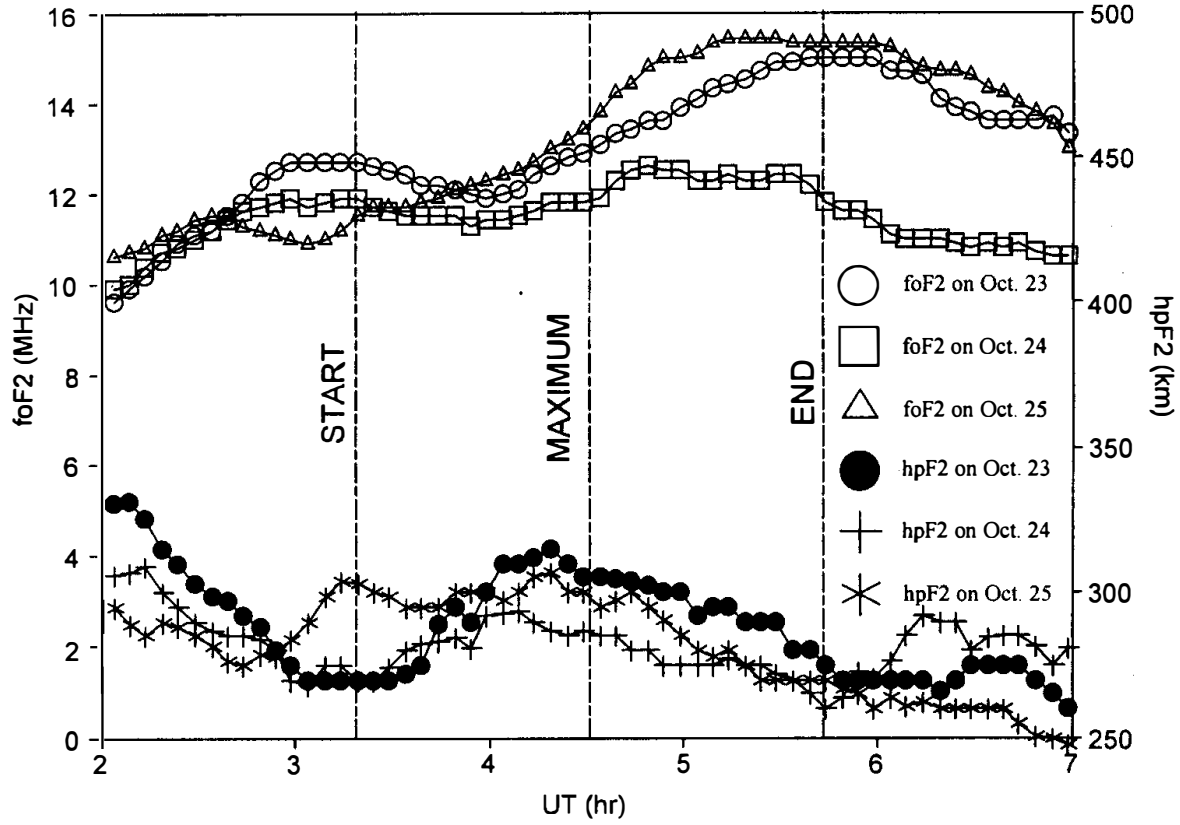

Fig. 2. foF2 and *hpF2* profiles with time on October 23, 24, and 25, 1995.

Table 1. Wigner-Ville Distribution Properties:

*P*1.	$W_x(t,\omega) = W_x^*(t,\omega)$	*Real*
*P*2.	$x(t) = x(-t) \Rightarrow W_x(t,\omega) = W_x(t,-\omega)$	*Even*
*P*3.	$x(t) \equiv 0, \forall t \notin (T_1,T_2) \Rightarrow W_x(t,\omega) \equiv 0, \forall t \notin (T_1,T_2)$	*Time support*
*P*4.	$X(\omega) \equiv 0, \forall \omega \notin (\Omega_1,\Omega_2) \Rightarrow W_x(t,\omega) \equiv 0, \forall \omega \notin (\Omega_1,\Omega_2)$	*Frequency support*
*P*5.	$y(t) = x(t-\tau) \Rightarrow W_y(t,\omega) = W_x(t-\tau,\omega)$	*Time shifts*
*P*6.	$Y(\omega) = X(\omega+\xi) \Rightarrow W_y(t,\omega) = W_x(t,\omega+\xi)$	*Frequency shifts*
*P*7.	$x(t) = f(t) \otimes_t q(t) \Rightarrow W_x(t,\omega) = W_f(t,\omega) \otimes_t W_q(t,\omega)$	*Convolution*
*P*8.	$x(t) = f(t)q(t) \Rightarrow W_x(t,\omega) = W_f(t,\omega) \otimes_\omega W_q(t,\omega)$	*Modulation*
*P*9.	$\begin{cases} x(t) = \dfrac{1}{2\pi x^*(0)} \int W_x(0.5t,\omega)\, e^{j\omega t} d\omega \\ X(\omega) = \dfrac{1}{X^*(0)} \int W_x(t,0.5\omega)\, e^{-j\omega t} dt \end{cases}$	*Signal recovery*
*P*10.	$\lvert x(t)\rvert^2 = \dfrac{1}{2\pi} \int W_x(t,\omega) d\omega$	*Instantaneous signal energy*
*P*11.	$\lvert X(\omega)\rvert^2 = \int W_x(t,\omega) dt$	*Power density*
*P*12.	$\Omega_x = \dfrac{\int \omega W_x(t,\omega) d\omega}{\int W_x(t,\omega) d\omega}$	*Instantaneous frequency*
*P*13.	$\tau_x = \dfrac{\int t W_x(t,\omega) dt}{\int W_x(t,\omega) dt}$	*Group delay*

3. THE WIGNER-VILLE DISTRIBUTION

The Wigner-Ville distribution (WVD) (Wigner, 1932), the origins of which lie in quantum statistical mechanics to describe the position and momentum of a particle, is the basis for all of the contemporary developments in time-frequency spectral analysis. Following the notation of Boudreaux-Bartels (1985), the WVD of an analytic signal $z(t)$ is expressed as:

$$W_z(t,\omega) = \int_{-\infty}^{\infty} z(t+\frac{1}{2}\tau) z^*(t-\frac{1}{2}\tau) e^{-j\omega\tau} d\tau$$

The properties of the WVD that distinguish it from other signal representations are summarized in Table 1. These properties are discussed in most overviews by Boudreaux-Bartels (1985). It is noted here that, unlike the Fourier transform, which determines the energy distribution of a signal only as a function of frequency, time-frequency representations can be applied to describe both the time and frequency characteristics of a signal. The WVD has been adapted to the case of discrete-time signals. One of the numerical procedures to evaluate the

WVD uses equally-spaced signal samples $z(nT)$ and FFT techniques to compute the value of the WVD along a discrete time-frequency grid (Boudreaux-Bartels, 1985), by which:

$$W_z(nT,\omega_\kappa) = 2T\sum_m z((n+m)T)z^*((n-m)T)e^{-j2\omega_\kappa mT}, \quad \text{where} \left(|\omega_\kappa| \le \frac{\pi}{2T}\right).$$

Most of the properties of the WVD carry directly over to the discrete-time case, but some cause problems associated with aliasing. It has been found that these aliasing components are not present if the signal is either oversampled by a factor of at least two or if it is analytic. However, the observed virtual heights are real and not analytic. To approach the Nyquist rate in the time-frequency spectral analysis of iso-frequency virtual height profiles with time, a transformation from real signals to analytic ones is required (Boashash, 1988). Furthermore, other than eliminating the problem of aliasing contributions, the Wigner-Ville distribution of an analytic signal is capable of avoiding the interaction items between positive and negative frequencies. The analytic signal $z(n)$ corresponding to a real signal $s(n)$ is defined in the time domain as:

$$z(n) = s(n) + jH[s(n)]$$

where $H[s(n)]$ represents the Hilbert transform of $s(n)$. Alternatively, the analytic signal can be defined in the frequency domain as:

$$Z(\kappa) = \begin{cases} S(\kappa), & \kappa = 0, \\ 2S(\kappa), & \kappa = 1,\ldots,\dfrac{N}{2}-1, \\ 0, & \text{otherwise}, \end{cases}$$

where $S(\kappa)$ for $\kappa = 0,\ldots N\text{-}1$ are the N-point discrete Fourier transform of $s(n)$.

4. A SEARCH FOR INDUCED ATMOSPHERIC GRAVITY WAVES

Chimonas and Hines (1970) suggested a theoretical concept for the production of atmospheric gravity waves induced by a solar eclipse. According to them, "as the lunar shadow sweeps at supersonic speed across the Earth, the cooling spot acts as a continuous source of gravity waves that build up into a bow wave, much as a rapidly moving boat produces a bow wave on the surface of the water it crosses." In the early eclipse observations, Walker *et al.* (1991) and Cheng (1993) observed at the same observatory in Chung-Li and applied the same maximum entropy method to the spectral analysis of iso-frequency virtual height profiles with time but obtained different periods of 30-33 min and 17-23 min, respectively, for the induced AGWs. Though the observed eclipses occurred on different days, namely on March 18, 1988 and September 23, 1987, the induced AGWs should have been consistent in period as discussed in the work of Chimonas and Hines (1971). In contrast, the results analyzed by the WVD, Figures 3 and 4 show the power wave spectra obtained using the maximum entropy method for various iso-frequency virtual height profiles with time on the eclipse day and the

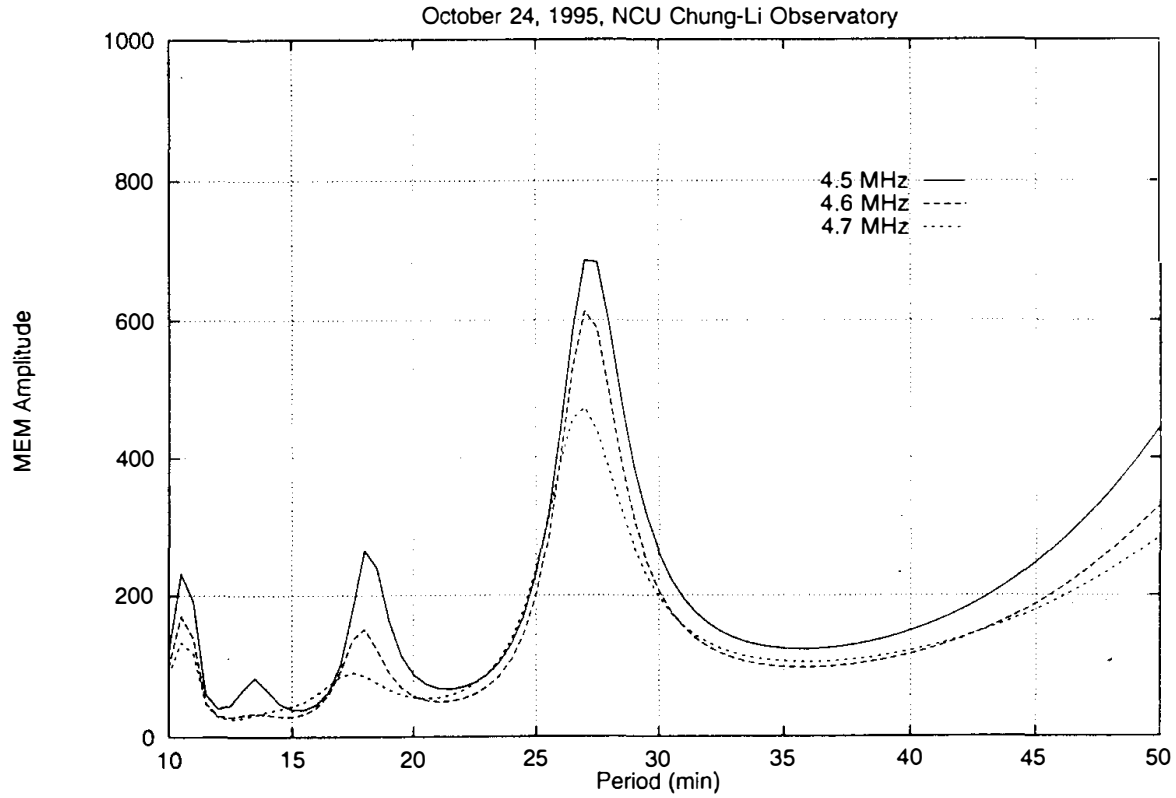

Fig. 3. The MEM spectra of iso-frequency virtual height profiles (at 4.5, 4.6, and 4.7 MHz) with time on the eclipse day.

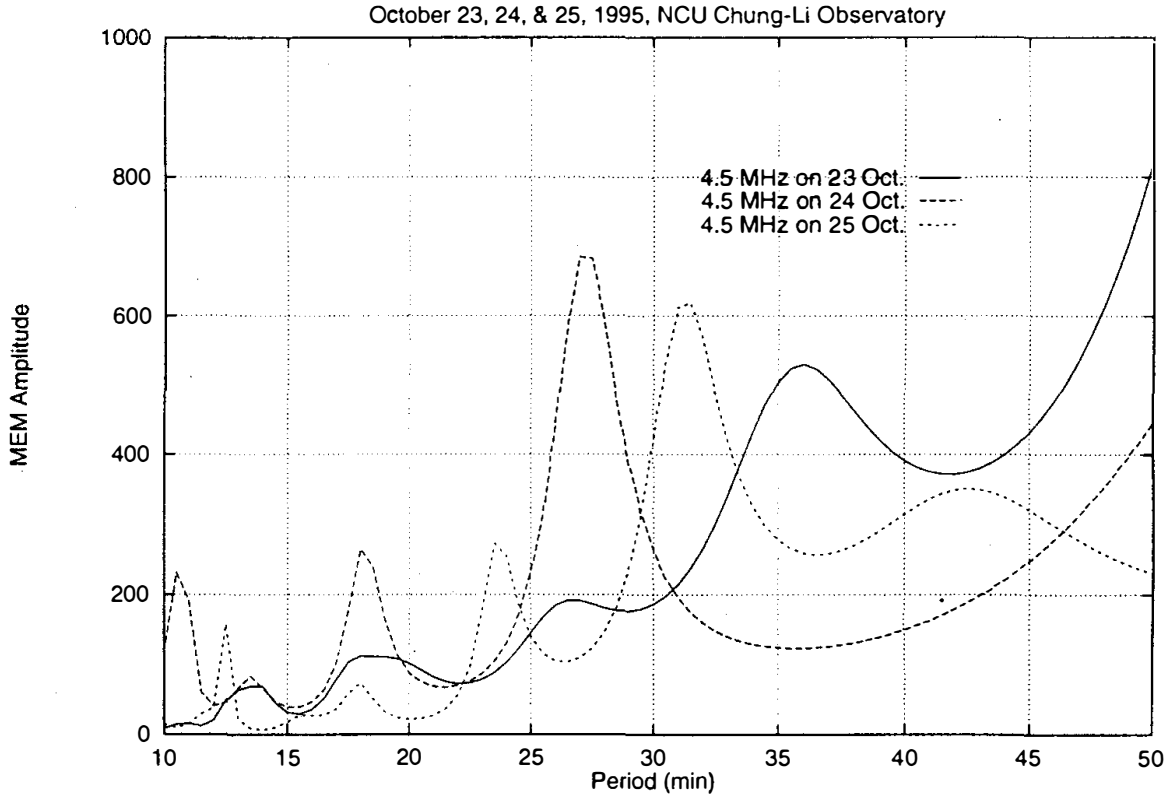

Fig. 4. MEM spectra of iso-frequency virtual height profiles (at 4.5 MHz) with time on the eclipse day and the two control days.

two control days first. As shown in Figure 3, three spectrum curves at 4.5, 4.6 and 4.7 MHz sounding frequencies indicate three main waves obtained on the eclipse day with the periods of 27, 18 and 11 min in which the first two of these are close to the wave periods observed by Walker *et al.* (1991) and Cheng (1993) individually. Furthermore, three wave amplitudes decrease with sounding frequency or altitude. Figure 4 shows that all three waves at 27, 18 and 11 min are much stronger on the eclipse day when compared with those on the two control days, but it is difficult to determine which is the induced AGW. From the suggestion of Chimonas and Hines (1970 and 1971), it is assumed that the induced AGW occurs during the eclipse period and continues to propagate for a few hours. With this non-stationary characteristic in use, in this study a period of 18.5 min for the induced AGW was obtained from the time-frequency spectral analysis based on the Wigner-Ville distribution. Figure 5 shows the WVD spectrum of the virtual height profile with time at a sounding frequency of 4.5 MHz. The strongest wave was obtained at a wave period of 27 min but occurred during a nonpredicted time from 1 UT to 6 UT. A weak wave with a period of 18.5 min can be identified from the start of the solar eclipse to a couple of hours after the end of the eclipse and is expected to be the induced AGW. The third wave with a period of 11 min also occurred during a nonpredicted time from 1 UT to 6 UT. In comparison, Figures 6 and 7 show the WVD spectra of the virtual height profiles with time at 4.5 MHz on the two control days separately. These plots clearly describe both the time and frequency characteristics of a signal spectrum. Figure 8 shows the corresponding three-dimensional perspectives of the 'windowed' WVD spectrum by a narrow period pass filter at 18.5 min for Figure 5. This 18.5 period AGW induced by the solar eclipse is consistent with the observations by Cheng (1993) and the early work reported by Davis and da Rosa (1970). Further evidence for the induced wave is shown by the *foE* and *foF1* profiles in Figure 1. Clearly, there are short ripples at ~20-min periods occurring after the eclipse maximum.

5. DISCUSSION AND CONCLUSIONS

In this study an automatic ionogram scaling algorithm incorporating fuzzy classification techniques has been developed and applied to a sequence of ionograms recorded on the eclipse day of October 24, 1995 at Chung-Li. The scaling results indicate significant depletions of *foE* and *foF1* during the eclipse time. Compared to the noneclipse time, the associated electron density was decreased by up to 33% at the eclipse maximum. Furthermore, to search for induced AGWs by a solar eclipse, the maximum entropy method has since been used to derive the associated wave frequency. The maximum entropy method, like the traditional Fourier transform, determines the energy distribution of a signal only as a function of frequency but, unfortunately, obscures the associated time characteristics. In contrast, the Wigner-Ville distribution yields both temporal and frequency information. In the *F1* and the lower part of the *F2*-layer, the time-frequency spectrum of the iso-frequency virtual height profiles in this study shows a weak wave with an 18.5-min period obtained at the predicted time from the start of the solar eclipse to a couple hours after the end of the eclipse. This weak wave may be blanked by other strong waves caused by other transport or thermal processes on the ionosphere, but it is suggested that it is the corresponding AGW induced by a solar eclipse. However, it is realized

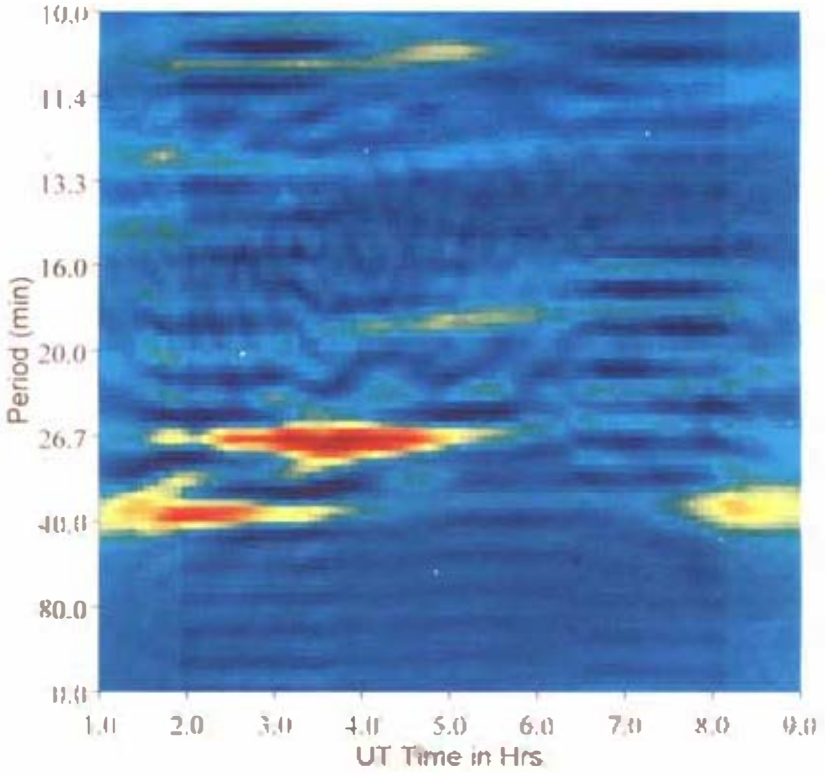

Fig. 5. WVD spectrum of the virtual height profile with time (at 4.5 MHz) on the eclipse day.

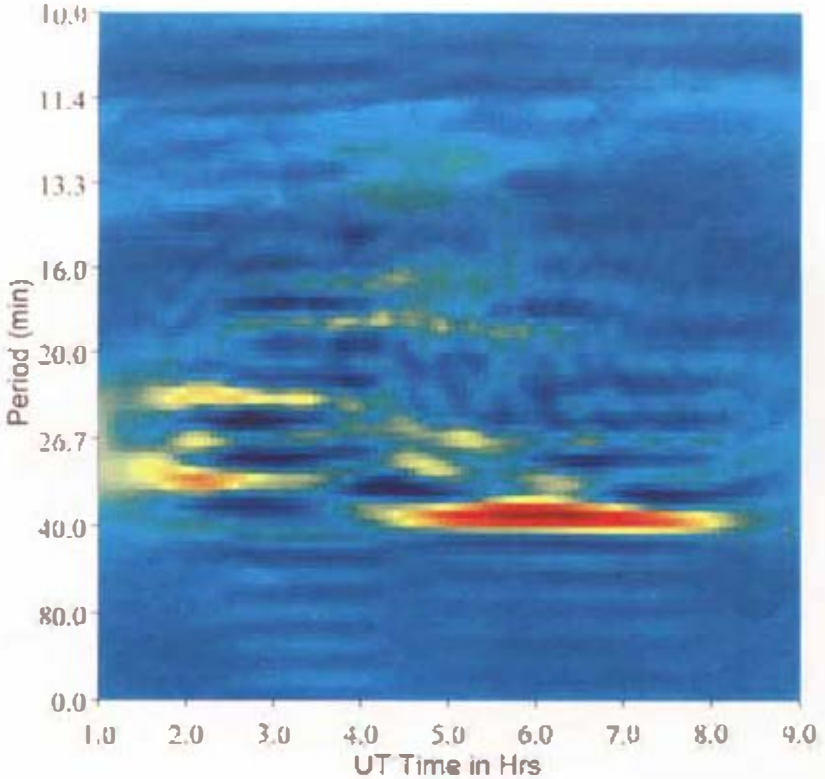

Fig. 6. WVD spectrum of the virtual height profile with time (at 4.5 MHz) on the previous control day.

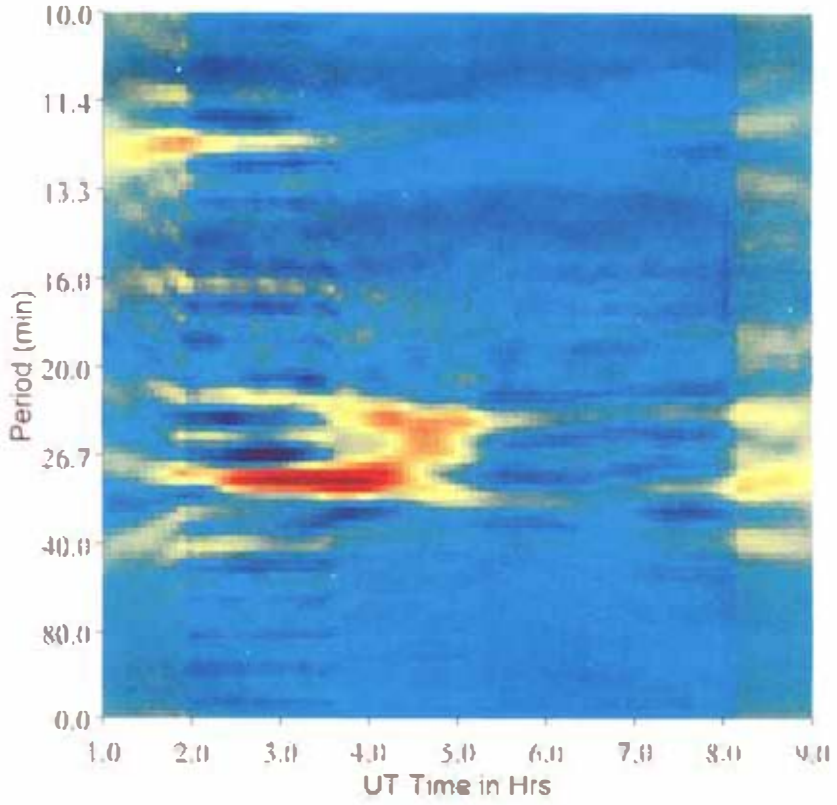

Fig. 7. WVD spectrum of the virtual height profile with time (at 4.5 MHz) on the next control day.

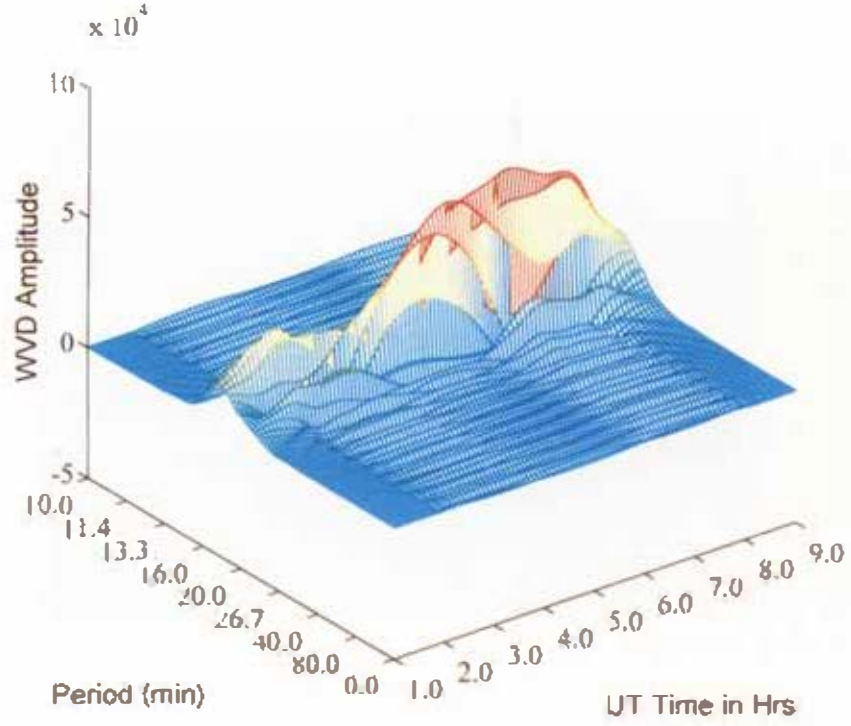

Fig. 8. Three-dimensional perspective of the windowed WVD spectrum of Figure 5.

that the present results, particularly those pertaining to observe the ionosphere using a single instrument at a particular observatory, cannot offer an ultimate confirmation. Future studies of the induced AGWs by a solar eclipse should be conducted in greater detail utilizing two or more instruments at a particular site or, even better, at various sites.

Acknowledgements This work has been supported by grants from the National Science Council under NSC85-2612-M-008-005 and NSC86-2111-M-008-005.

REFERENCES

Bibl, K. and B. W. Reinisch, 1978: The universal digital ionosonde. *Radio Sci.*, **13**, 519-530.

Boashash, B., 1988: Note on the use of the Wigner distribution for time-frequency signal analysis, IEEE Trans. Acoust., Speech, Signal Processing, **36**, 1518-1521.

Boudreaux-Bartels, G.F., 1985: Time-varying signal processing using the Wigner distribution time-frequency signal representation. In: Advances in Geophysical Data Processing, JAI Press, **2**, 33-79.

Chimonas, G., and C. O. Hines, 1970: Atmospheric gravity waves induced by a solar eclipse, 1. *J. Geophy. Res.*, **75**, 875.

Chimonas, G., and C. O. Hines, 1971: Atmospheric gravity waves induced by a solar eclipse, 2. *J. Geophy. Res.*, **76**, 7003-7005.

Cheng, K., 1992: Ionospheric transient variations around equatorial anomaly crest region, Ph.D. dissertation, Dept. of Electrical Engineering, National Taiwan University, Taipei, Taiwan.

Davies, K.,1982: Proc. Indian Nat. Sci. Acad., 48A, 342pp.

Davis, M. J. and A. V. da Rosa, 1970: Possible detection of atmospheric gravity waves generated by the solar eclipse. *Nature*, **226**, 1123.

McNamara, L. F. and J. E. Titheridge, 1977: Numerical ionograms for comparing methods of N(h) analysis. IPS Series R Reports X-5.

Reinisch, B. W., 1986: New techniques in ground-based ionospheric sounding and studies. *Radio Sci.*, **21,** 331-341.

Tsai, L.-C., J. Y. Liu and F. T. Berkey, 1996: Automatic ionogram trace identification using fuzzy classification techniques, Paper G5, URSI 25th General Assembly, Lille, France.

Ulrych, T. J. and T. N. Bishop, 1975: Maximum entropy spectral analysis and autoregressive decomposition. *Rev. Geophys. Space Phys.*, **13**, 183-200.

Walker, G. O., T. Y. Y. Li, Y. W. Wong, T. Kikuchi and Y. N. Huang, 1991: Ionospheric and geomagnetic effects of the solar eclipse of 18 March 1988 in East Asia. *J. Atmos. Terr. Phys.*, **53**, 25-37.

Wigner, E.P., 1932: On the quantum correction for thermo-dynamic equilibrium. *Phys. Rev.*, 4040 **40,** 748-759.